11-2014

Multiscale Bed Form Interactions and Their Implications for the Abruptness and Stability of the Downwind Dune Field Margin at White Sands, New Mexico, USA

Jon D. Pelletier

Douglas J. Jerolmack
University of Pennsylvania, sediment@sas.upenn.edu

Recommended Citation
Pelletier, J. D., & Jerolmack, D. J. (2014). Multiscale Bed Form Interactions and Their Implications for the Abruptness and Stability of the Downwind Dune Field Margin at White Sands, New Mexico, USA. *Journal of Geophysical Research: Earth Surface, 119* (11), 2396-2411. http://dx.doi.org/10.1002/2014JF003210

Multiscale Bed Form Interactions and Their Implications for the Abruptness and Stability of the Downwind Dune Field Margin at White Sands, New Mexico, USA

Abstract
The downwind margin of White Sands dune field is an abrupt transition from mobile aeolian dunes to a dune-free vegetated surface. This margin is also relatively stable; over the past 60 years it has migrated several times more slowly than the slowest dunes within the dune field, resulting in a zone of dune coalescence, aggradation, and, along most of the margin, development of a dune complex (i.e., dunes superimposed on draas). Repeat terrestrial laser scanning surveys conducted over a 3 month period demonstrate that sediment fluxes within the dune complex decrease on approach to the margin. Computational fluid dynamics modeling indicates that this decrease is due, in part, to a decrease in mean turbulent bed shear stress on the lee side of the dune complex as a result of flow line divergence or sheltering of the lee-side dunes by the stoss side of the dune complex. Conservation of mass demands that this decrease in bed shear stress causes aggradation. We speculate that aggradation on the lee side of the dune complex further enhances the sheltering effect in a positive feedback, contributing to the growth and/or maintenance of the dune complex and a relatively abrupt and stable dune field margin. Our model and data add to a growing body of evidence that aeolian dune field patterns are influenced by feedbacks that occur at scales larger than individual dunes.

Keywords
aeolian dunes, terrestrial laser scanning (TLS), computational fluid dynamics (CFD)

Disciplines
Earth Sciences | Environmental Sciences | Physical Sciences and Mathematics | Sedimentology

AGU PUBLICATIONS

JGR

Journal of Geophysical Research: Earth Surface

RESEARCH ARTICLE
10.1002/2014JF003210

Key Points:
- The downwind dune field margin at White Sands is remarkably stable and abrupt
- Combining TLS changes, CFD modeling, and field studies is powerful
- Coupling of topography, flow, and sediment transport acts to maintain the margin

Correspondence to:
J. D. Pelletier,
jdpellet@email.arizona.edu

Citation:
Pelletier, J. D., and D. J. Jerolmack (2014), Multiscale bed form interactions and their implications for the abruptness and stability of the downwind dune field margin at White Sands, New Mexico, USA, *J. Geophys. Res. Earth Surf.*, *119*, 2396–2411, doi:10.1002/2014JF003210.

Received 14 MAY 2014
Accepted 5 OCT 2014
Accepted article online 9 OCT 2014
Published online 8 NOV 2014

Multiscale bed form interactions and their implications for the abruptness and stability of the downwind dune field margin at White Sands, New Mexico, USA

Jon D. Pelletier[1] and Douglas J. Jerolmack[2]

[1]Department of Geosciences, University of Arizona, Tucson, Arizona, USA, [2]Department of Earth and Environmental Science, University of Pennsylvania, Philadelphia, Pennsylvania, USA

Abstract The downwind margin of White Sands dune field is an abrupt transition from mobile aeolian dunes to a dune-free vegetated surface. This margin is also relatively stable; over the past 60 years it has migrated several times more slowly than the slowest dunes within the dune field, resulting in a zone of dune coalescence, aggradation, and, along most of the margin, development of a dune complex (i.e., dunes superimposed on draas). Repeat terrestrial laser scanning surveys conducted over a 3 month period demonstrate that sediment fluxes within the dune complex decrease on approach to the margin. Computational fluid dynamics modeling indicates that this decrease is due, in part, to a decrease in mean turbulent bed shear stress on the lee side of the dune complex as a result of flow line divergence or sheltering of the lee-side dunes by the stoss side of the dune complex. Conservation of mass demands that this decrease in bed shear stress causes aggradation. We speculate that aggradation on the lee side of the dune complex further enhances the sheltering effect in a positive feedback, contributing to the growth and/or maintenance of the dune complex and a relatively abrupt and stable dune field margin. Our model and data add to a growing body of evidence that aeolian dune field patterns are influenced by feedbacks that occur at scales larger than individual dunes.

1. Introduction

The evolution of aeolian dune fields has received renewed attention in the geomorphic and planetary science communities in recent years, stimulated by the availability of new multitemporal airborne laser swath mapping and terrestrial laser scanning (TLS) data sets [*Nagihara et al.,* 2004; *Jerolmack et al.*, 2012; *Feagin et al.*, 2012; *Pelletier*, 2013; *Baitis et al.*, 2014], advances in process-based numerical modeling [*Andreotti et al.,* 2002a, 2002b; *Hersen,* 2004; *Hersen et al.*, 2004; *Hersen and Douady*, 2005; *Herrmann et al.*, 2005, 2008; *Durán et al.*, 2005; *Katsuki et al.*, 2005; *Pelletier*, 2009; *Diniega et al.*, 2010], and imaging of dune fields on Mars and Titan [e.g., *Parteli and Herrmann*, 2007; *Bourke*, 2010; *Bridges et al.*, 2012]. One essential part of this renaissance has been a recognition of the importance of multiscale interactions (among dunes; among ripples, dunes and draas; and between dunes and their underlying or surrounding topography) on dune evolution [e.g., *Hersen et al.*, 2004; *Pelletier*, 2009; *Diniega et al.*, 2010; *Durán et al.*, 2010; *Jerolmack et al.*, 2012; *Worman et al.*, 2013; *Baitis et al.*, 2014].

Multitemporal lidar data analysis is a particularly powerful tool for demonstrating the importance of multiscale interactions on dune geometries and migration rates. At White Sands dune field in New Mexico, for example, aeolian sediment fluxes and mean dune heights are both at a maximum at the upwind margin of the dune field and decrease, to first order, with increasing distance downwind. These patterns have alternatively been attributed to the response of the atmospheric boundary layer (ABL) to spatial variations in dune size [*Jerolmack et al.*, 2012] and to the influence of long-wavelength topographic variations on surface sediment moisture and hence mobility [*Baitis et al.*, 2014]. *Jerolmack et al.* [2012] demonstrated that spatial variations in dune size, including the transition from the absence to presence of dunes at the upwind margin of the dune field, trigger adjustments in the ABL that result in a maximum sediment flux at the upwind margin and a decrease in sediment flux with increasing distance downwind. *Jerolmack et al.* [2012] demonstrate the potential importance of boundary conditions and/or sharp gradients on dune evolution far from such boundaries/gradients. *Baitis et al.* [2014] proposed that dune field properties are also controlled by the two

most prominent paleoshoreline scarps in the dune field: one coincident with the upwind margin and the other located 6–7 km downwind from the margin. *Baitis et al.* [2014] argued that sediments comprising the crests of these scarps are relatively dry, thus resulting in higher sediment fluxes for otherwise similar wind forcing conditions. Remote sensing studies of surface moisture indeed indicate drier-than-average conditions at the crests of these two scarps, a fact that *Scheidt et al.* [2010] associated with an approximately 20% decrease in the threshold wind velocity for entrainment compared with wetter-than-average areas of the dune field.

The *Jerolmack et al.* [2012] and *Baitis et al.* [2014] studies did not include the downwind margin of the dune field, a boundary condition/gradient just as abrupt as the upwind margin that data suggest behaves in an unusual way. A greater understanding of the behavior of this margin may contribute to our understanding of dune evolution, in general. The downwind dune field margin of White Sands is, in most places, an abrupt transition from mobile dunes to a dune-free vegetated surface. In this paper we focus on the downwind margin and ask the following: can gradients in parameters that influence aeolian transport associated with the downwind margin have effects on dunes located upwind of the margin? In addition to its abruptness, the downwind margin at White Sands has been relatively stable over the past 60 years (Figure 1). A comparison of coregistered images acquired in 1942 and 2003 indicates that the downwind margin (identified using surface reflectivity and/or the shadow associated with the lee side of the terminal dune) in the vicinity of the White Sands National Monument headquarters shown in Figure 1 has migrated at an average rate of 0.4 ± 0.1 m a^{-1} during this time interval. The migration of this margin exhibits significant spatial variability, with some more heavily vegetated portions not migrating at all (within uncertainty) and other portions migrating by more than 100 m over the 60 year time interval. Dunes within the dune field migrate at rates from 2–10 m a^{-1} [*McKee and Douglass*, 1971; *Ewing and Kocurek*, 2010]. As such, the downwind margin has migrated several times more slowly than the slowest dunes within the dune field. The relatively low migration rate of the downwind margin contrasts with the findings of *Laick* [2001], who concluded that the margin near the Monument headquarters migrated at an average rate of 3.9 m a^{-1} between 1987 and 2000. The reason for the discrepancy between our results and those of *Laick* [2001] is unclear, but *Laick* [2001] emphasized the uncertainty of his analysis, which he attributed to the limited time interval he considered and his use of variable-resolution imagery.

According to conservation of mass, the decrease in aeolian sediment flux on approach to the margin, suggested by the difference in migration rates between the downwind margin and dunes within the dune field, and further documented in this paper using repeat terrestrial laser scanning (TLS), results in a zone of aggradation just upwind of the margin. The downwind margin of White Sands coincides along most of its length with a dune complex, i.e., dunes superimposed on draas (Figure 1a). In this paper we demonstrate that the presence of the dune complex results in an aerodynamic sheltering effect and a resulting decrease in sediment flux on the lee side of the dune complex. We speculate that the zone of aggradation required by the decrease in sediment flux on approach to the margin contributes to the growth and/or maintenance of the dune complex, which in turn contributes to the abruptness and stability of the downwind margin in a positive feedback.

2. Study Area and Conceptual Model

The White Sands dune field occupies approximately 400 km^2 of the Tularosa Basin and contains dunes composed of gypsum sand eroded from evaporite deposits on the floor of the former Pleistocene Lake Otero [e.g., *McKee*, 1966; *Langford*, 2003]. The basin is bounded by the San Andres Mountains to the west and the Sacramento Mountains to the east. The dune field sits in the south central portion of the basin, approximately equidistant from these mountain ranges. Dunes extend for up to 15 km in the predominant transport direction, approximately 65° [*Reitz et al.*, 2010]. The dune field is made up of dunes composed of mobile sand, which migrate over a relatively immobile substrate of wet sand that is maintained by a shallow groundwater table. The flat, typically moist surfaces between mobile dunes are called interdunes and show stratigraphic evidence of persistent dune migration and accumulation [*Kocurek et al.*, 2007]. The dune field terminates abruptly in a sinuous line that ranges in distance from the upwind margin, $x = 12$–15 km. At the upwind margin there is almost no vegetation on the dunes or interdunes. Moving downwind, moist interdunes are the first to be populated with plants, whose density increases with distance downwind. Aerial

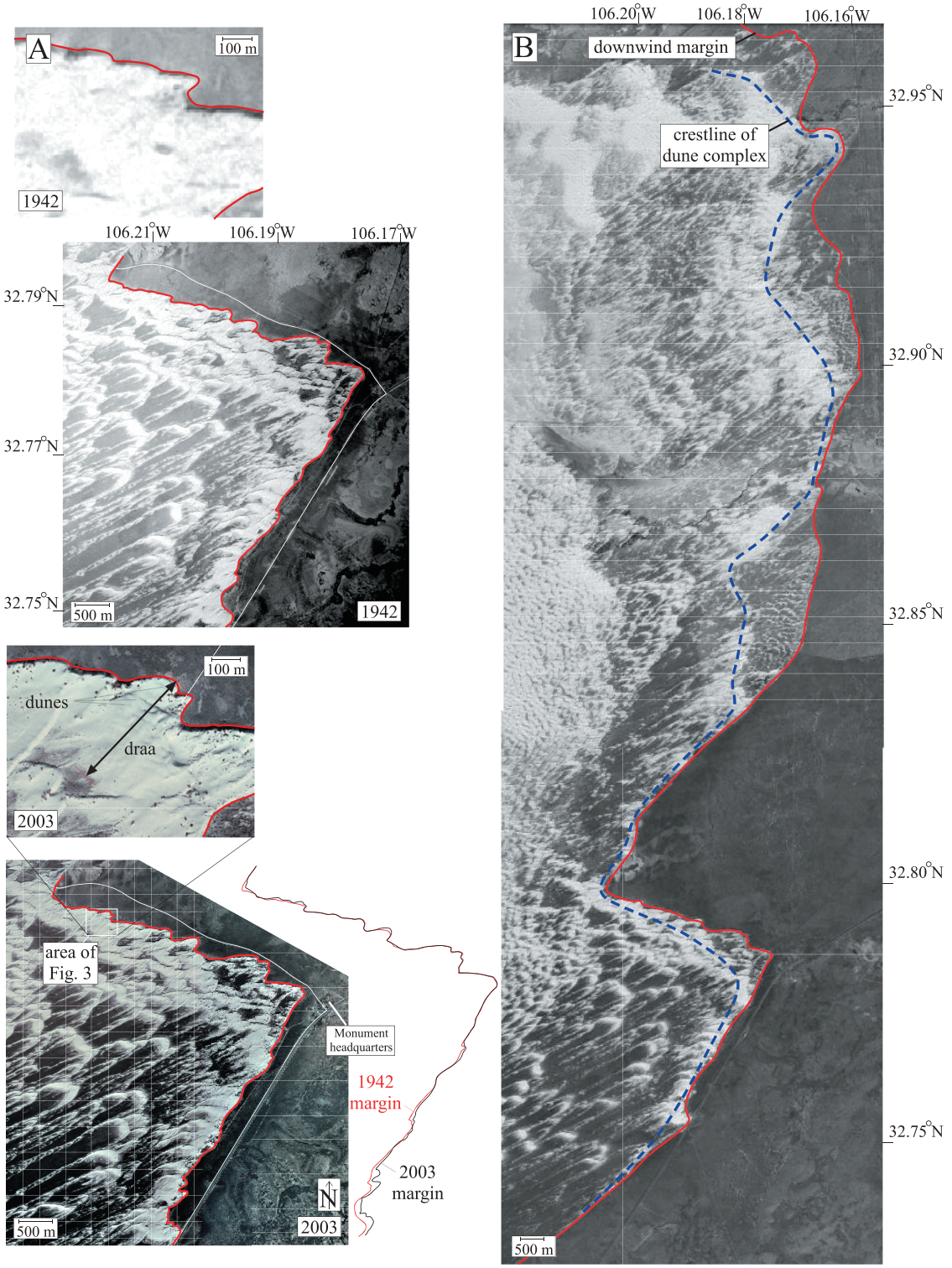

Figure 1. (a) Aerial photographic analysis of the migration of the portion of the downwind dune field margin at White Sands located near the Monument headquarters, from 1942 to 2003. Inset images show the portion of the margin chosen for TLS surveying. (b) Map of the downwind margin, illustrating the close association between the dune complexes (shown as dotted blue curve) and downwind margin (solid red curve).

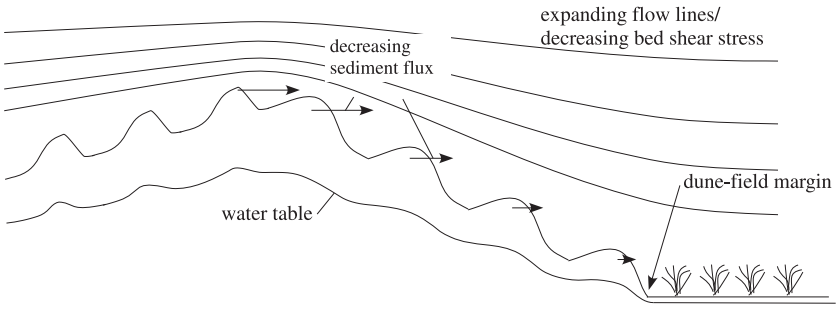

Figure 2. Schematic diagram of the downwind dune field margin at White Sands.

photographs and field observations show that plant density on dunes is negligible until $x \approx 7$ km, at which point plants begin to colonize the migrating dunes [*Reitz et al.*, 2010] and the dunes transition from forward pointing (unvegetated) barchans to (vegetated) parabolics with trailing arms.

The dunes just upwind of the downwind margin are, in most places, a dune complex (shown schematically in cross section in Figure 2), i.e., a set of small (i.e., ≈ 50 m spacing) dunes, often with both barchanoid and parabolic forms present, superimposed on larger (i.e., ≈ 400 m in length) draas that are primarily parabolic in form. Such dune complexes have been documented elsewhere [*Brookfield*, 1977; *Havholm and Kocurek*, 1988; *Langford et al.*, 2008], but we lack a mechanistic understanding of how the large-scale topography of the draa influences the migration of the dunes superimposed on them. This study is designed to fill that gap.

The schematic diagram in Figure 2 emphasizes three processes/mechanisms that may influence spatial variations in sediment flux within the dune complex and the abruptness and stability of the adjacent downwind dune field margin. First, the large-scale topography of the dune complex may cause flow line divergence on the lee side of the complex that influences sediment fluxes (illustrated in Figure 2 using arrows of decreasing length on approach to the margin). Second, the long-wavelength topography of the dune complex may influence surface sediment moisture and hence sediment mobility via interactions among topography and groundwater flow. In locations where infiltration is relatively uniform, the water table is expected to be relatively deep (and the surface sediments relatively dry and mobile) beneath areas with the largest topographic convexity (since groundwater fluxes are driven by topographic gradients). Third, the transition from a relatively dune-covered unvegetated surface to a dune-free vegetated surface potentially represents a rough-to-smooth aerodynamic transition analogous to the smooth-to-rough aerodynamic transition that *Jerolmack et al.* [2012] argued controls the abruptness of the upwind margin at White Sands. Such roughness transitions can trigger shear stress overshoots/undershoots in their vicinity that can control sediment fluxes.

In this paper we first demonstrate a systematic decrease in aeolian sediment flux on the lee side of the dune complex on approach to the margin using an analysis of repeat terrestrial laser scanning (TLS) data. As part of that analysis we show how high-resolution sediment flux data can be inferred from topographic change data via integration along predominant sand transport pathways. Second, we test alternative hypotheses for the mechanisms responsible for controlling the sediment flux decrease on approach to the margin using a computational fluid dynamics (CFD) model. The CFD model predicts spatial variations in sediment flux that match measured sediment fluxes relatively well without incorporating the effects of spatially variable surface sediment moisture or the effects of a possible rough-to-smooth transition associated with the downwind margin, suggesting that the dominant effect in controlling the decrease in sediment flux on approach to the margin is the aerodynamic sheltering effect of the stoss side and crest of the dune complex.

3. Methods

3.1. Terrestrial Laser Scanning and Creation of a DEM-of-Difference

We conducted terrestrial laser scanning (TLS) surveys of a segment of the downwind dune field margin on 7 March 2013 and again on 4 June 2013 (Figure 3; location of TLS survey site shown in Figure 1; 32.791°N, 106.207°W). The portion of the dune field margin we surveyed was chosen based on its accessibility and the

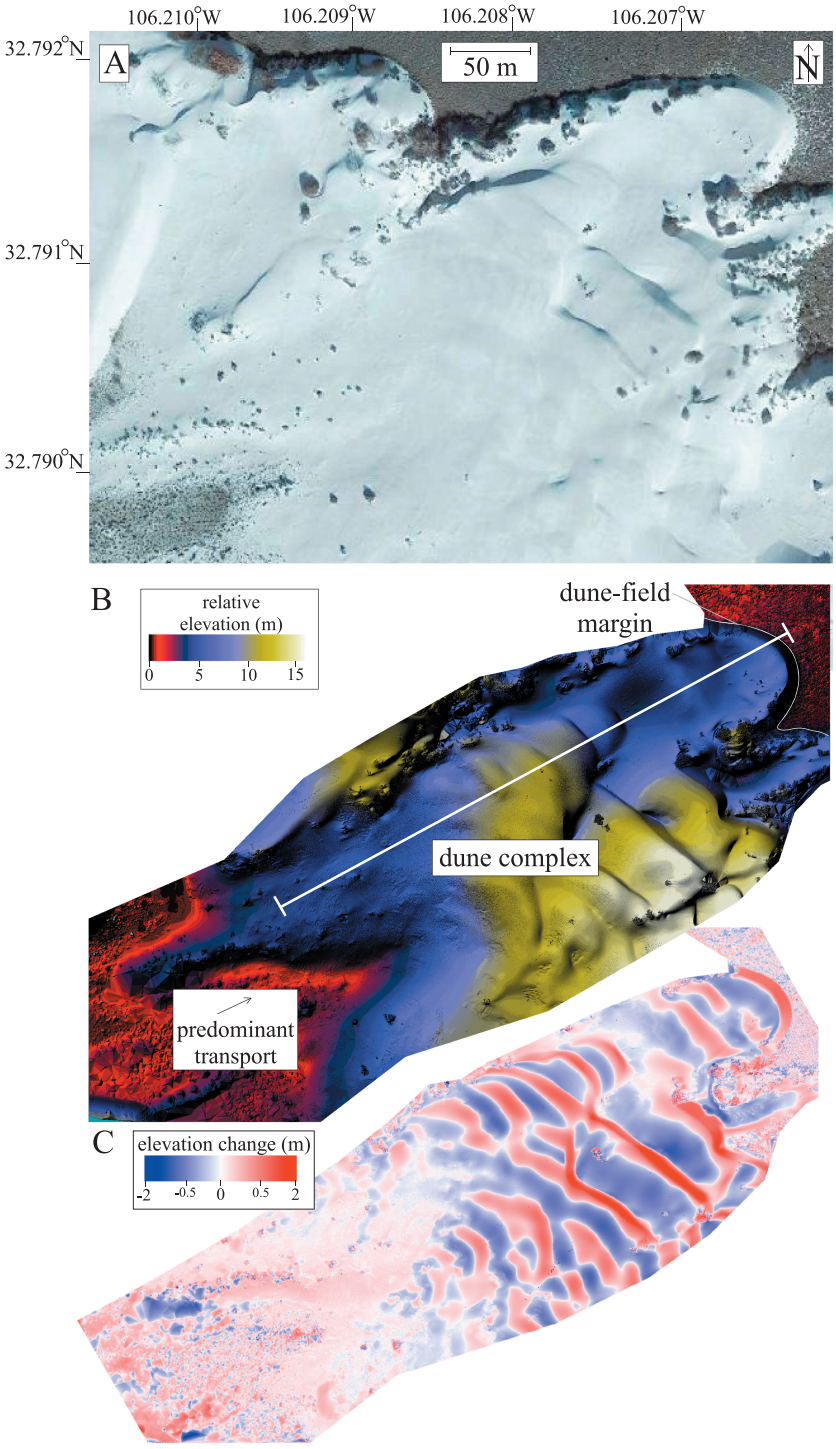

Figure 3. (a) Georectified 2013 aerial photograph of the dune complex and (b and c) color maps of the elevation (shaded relief included, with illumination angle from the northwest) and erosion/deposition (Figure 3b) resulting from the TLS surveys of 7 March and 4 June 2013.

relative absence of vegetation (which improves the accuracy of the bare-ground digital elevation model (DEM) derived from TLS data).

A Leica C10 scanner was used to acquire TLS data using stations located approximately 20 m apart. Such spacing required 27 scan stations to cover the survey area illustrated in Figure 3. The Leica C10 has an

inherent surface model accuracy of 0.002 m under ideal conditions (i.e., a vegetation-free surface) [*Hodge et al.*, 2009]. A minimum of three Leica targets were used to register each scan to the others to create a unified point cloud (registration errors < 0.005 m). Real-Time Kinematic Global Positioning System (GPS) surveys were performed enabling absolute georeferencing of each unified point cloud (errors < 0.02 m).

Vegetation points within the unified point cloud were partially removed by retaining only the lowest returns within each 0.05 m × 0.05 m domain. These points were then converted to a Triangular Irregular Network (TIN). We interpolated each TIN to a 0.05 m pixel^{-1} raster/DEM. A DEM-of-Difference (DoD) was created by differencing the two precisely coregistered bare-ground DEMs. Vegetation cover on the dunes is extremely sparse but becomes dense in the interdune areas and on the vegetated surface downwind of the margin. As such, the DoD illustrated in Figure 3b is most accurate on the dune complex itself due to the sparse vegetation cover. In contrast, some of the apparent topographic change on the vegetated surfaces upwind and downwind of the dune complex is a result of not completely filtering out the vegetation from the point cloud in areas of dense vegetation.

The DoD that resulted from differencing the DEMs acquired on 7 March and 4 June 2013 quantifies the erosion or deposition rate (in units of $\mathrm{L\,T^{-1}}$) over the approximately 3 month time interval between the two surveys. Three months is a relatively short period of time in which to measure dune activity, but aeolian transport at White Sands (as elsewhere in the western US) occurs primarily in the spring months. As such, our March–June survey covers the most important 3 months of the year in terms of dune activity. We extracted a topographic profile through the survey area along the predominant direction of aeolian sediment transport (profile location shown in Figure 3b) and integrated the topographic change spatially along the profile (starting 50 m downwind from the margin, where the sediment flux can be assumed to be negligible) to obtain the volumetric unit sediment flux (in units of $\mathrm{L^2\,T^{-1}}$). The Exner equation [*Exner,* 1920, 1925], expressed in a finite-difference volumetric form, states

$$\frac{\Delta h_i}{\Delta t} = -\frac{1}{1-\lambda}\frac{\Delta q_s}{\Delta x}, \tag{1}$$

where Δh_i is the change in ground surface elevation over a time interval Δt, λ is the sediment porosity (in the range of 0.23–0.30 for White Sands [*Ahlbrandt*, 1979]; 0.25 is assumed here), q_s is the volumetric unit sediment flux, and Δx is the distance between sample points in the along-wind direction. Equation (1) shows that given values for the erosion/deposition rate, i.e., $\Delta h_i/\Delta t$, along a profile (where i is an index of discrete points along the profile), the unit volumetric sediment flux can be determined via Euler integration along the profile, i.e.,

$$q_s = -(1-\lambda)\sum_{i=1}^{n}\frac{\Delta h_i}{\Delta t}\Delta x + q_0 \tag{2}$$

where n is the number of points along the profile. The constant of integration q_0 is constrained by assuming q_s is zero far downwind of the margin (where sediment flux is negligible due to the dense vegetation cover of the surface).

3.2. Estimation of Effective/Apparent Aerodynamic Roughness Length

CFD modeling of flow over dunes requires an input DEM (or a topographic profile, if the model is two dimensional (2-D)) and an estimate of the effective/apparent aerodynamic roughness length(s), z_0 (which can vary spatially). Typical DEM data for dunes obtained from TLS or ALS are ~0.1–1 m pixel^{-1} resolution; hence, variations in elevation and/or topographic roughness at scales larger than ~0.1–1 m are captured by the input DEM while smaller-scale variations are not. The value(s) of z_0 input to the CFD model must include the effects of roughness at scales smaller than ~0.1–1 m, which includes most ripples and the drag induced by saltation. We refer to such small-scale effective roughness lengths as ripple-scale effective roughness lengths in this paper (denoted z_{0r}).

Two common methods exist for estimating z_{0r} values: the modified Charnock relation of *Sherman* [1992] and *Sherman and Farrell* [2008] and direct measurement using a portable tower with multiple anemometers located at variable distances from the ground. In this paper we use both methods. The modified Charnock relation is

$$z_{0r} = \frac{d_{50}}{15} + C_m\frac{(u_* - u_{*_t})^2}{g}, \tag{3}$$

where z_{0r} is the ripple-scale effective aerodynamic roughness length, C_m is an empirical coefficient, u_* is the shear velocity, u_{*t} is the threshold shear velocity (equal to approximately 0.32 m s^{-1} at White Sands assuming a median grain size of 0.4 mm and grain density of 2600 kg m^{-3}), and g is the acceleration due to gravity. *Sherman and Farrell* [2008] obtained $C_m = 0.132$ by fitting measured velocity profiles from the literature over a range of shear velocities from 0.09 to 1.25 m s^{-1} and obtained z_{0r} values from 0.0001 m to 0.0121 m. The first term on the right side of equation (3) is the grain-scale roughness, and the second term includes the effects of saltation-induced roughness. During vigorous saltation, the second term on the right side of equation (3) is typically 1–3 orders of magnitude larger than the first term.

The modified Charnock relation applies only to erodible beds with no vegetation. In order to quantify the effects of a rough-to-smooth transition at the downwind margin (where dunes transition to a dune-free vegetated surface), it is necessary to directly measure the z_{0r} value of a surface covered with plants of the same type as that found immediately downwind of the margin, i.e., the saltbush/alkali sacaton association, which has plant heights of approximately 0.3 m as measured in the field. We measured wind velocity profiles and inferred z_{0r} and u_* values from those profiles in an interdune area with the same saltbush/alkali sacaton association and similar density to that of the vegetated surface downwind of the dune field margin (Figure 4a). We should emphasize that the parabolic dune illustrated in Figure 4a is not the same dune surveyed by TLS. We chose not to measure z_{0r} values downwind of the TLS survey site or dune field margin itself because of the likelihood that the dune complex would influence z_{0r} values for tens to hundreds of meters downwind from the margin.

Figure 4 illustrates the six locations where z_{0r} values were measured on 10 March 2013. Winds were relatively calm (3.7–7.6 m s^{-1} at 2.18 m above the ground, with most values in the 4–6 m s^{-1} range and no visible transport); hence, saltation-induced roughness effects are not included in these data. Wind speeds were measured simultaneously at four heights (0.2 m, 0.56 m, 1.22 m, and 2.18 m) using standard cup anemometers (Inspeed brand) logging data simultaneously to a PC. The wind tower was placed at six stations along a vegetation gradient for 10 min per station; z_{0r} and u_* values were obtained by fitting 1 min averaged wind speeds to the law of the wall, i.e., [*Bagnold*, 1941]

$$u(z) = \frac{u_*}{\kappa} \ln\left(\frac{z}{z_{0r}}\right), \tag{4}$$

where u is the wind velocity, z is the elevation above the bed, and κ is the von Karman constant (0.41), for a total of 60 measured values of z_{0r} and u_*. The 1σ uncertainty in each z_{0r} and u_* values was quantified based on 1σ uncertainty values in the fit parameters.

An estimate of the dune-scale effective aerodynamic roughness length, z_{0d}, is also needed since we used CFD models to predict the response of the ABL to the downwind margin, the roughness of which is dominated by dunes on the upwind side and vegetation on the downwind side. To estimate the dune-scale effective aerodynamic roughness length, z_{0d}, upwind of the margin, we used a reference value of z_{0r} appropriate for vigorous saltation conditions (i.e., 0.01 m) together with the empirical relationship developed by *Jacobs* [1989] for flow over a wavy surface:

$$\frac{z_{0d}}{z_{0r}} = \exp\left(\frac{1}{2}\left(S \ln\left(\frac{L}{z_{0r}}\right)\right)^2\right) \tag{5}$$

where z_{0r} is the ripple-scale roughness length (i.e., the roughness that the surface would have without the dunes, i.e., with only microtopographic variations such as ripples), L is the half-length of the dunes at the half-height position, and S is the maximum slope. There is significant uncertainty associated with applying equation (5) to predicting the dune-scale effective roughness length because equation (5) was developed for symmetric bed forms. As such, it is not inherently obvious whether the S input into equation (5) should be the maximum slope of the stoss side of the dune, the maximum slope of the lee side, or some average of the two. J. D. Pelletier (Controls on the large-scale spatial variations of dune field properties in the barchanoid portion of White Sands dune field, New Mexico, *Journal of Geophysical Research*, in review, 2014) tested the predictions of equation (5) against CFD model calculations and found the predictions to be most accurate when the maximum slope of the stoss side of the bed form was used for S.

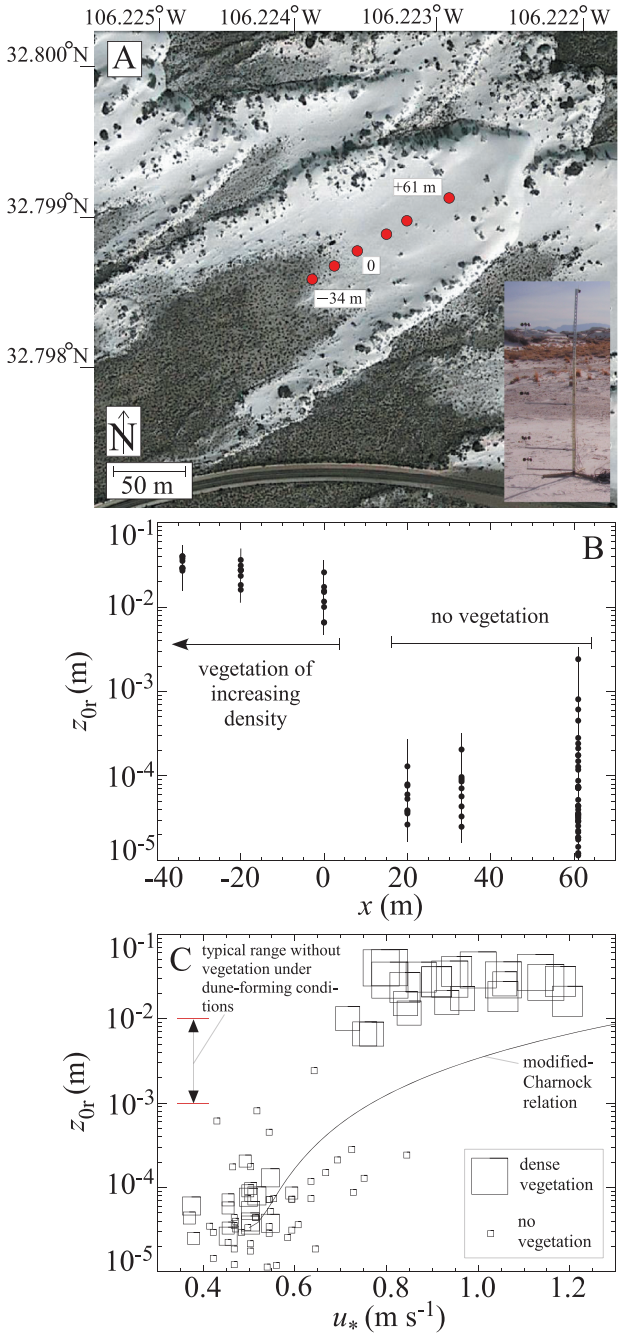

Figure 4. Measurements of the ripple-scale effective aerodynamic roughness length, z_{0r}, determined from wind velocity profiles acquired across the vegetation cover gradient associated with the interdune-to-stoss-slope transition in a parabolic dune at White Sands. (a) Measurement locations (shown as red circles). Inset photo shows the portable wind tower we used. Note that this parabolic dune is not the same dune as the dune complex surveyed by TLS. (b) Plot of z_{0r} as a function of distance downwind from the vegetation boundary (negative values indicate positions upwind of the vegetation boundary). (c) Plot of z_{0r} versus u_* using the same data as Figure 4b, along with the predictions of the modified Charnock relation of *Sherman* [1992] and *Sherman and Farrell* [2008] (which only applies to unvegetated surfaces). Data points collected in areas of higher vegetation density (or closer to areas of higher vegetation density) are shown using larger squares.

3.3. Numerical Modeling

The goals of the numerical modeling were twofold: (1) to predict the spatial variations of aeolian sediment flux over the dune complex and compare the results to TLS-based measurements of flux over the 3 month measurement period and (2) to quantify patterns of bed shear stress associated with idealized roughness transitions in order to test the hypothesis that the abruptness and stability of the downwind margin is controlled primarily by a rough-to-smooth aerodynamic transition.

To predict the spatial variations in bed shear stresses and associated aeolian sediment fluxes over the dune complex adjacent to the dune margin, we used the PHOENICS CFD modeling package [*Ludwig*, 2011]. PHOENICS uses a finite-volume scheme to solve simultaneously for the pressure and flow velocity in boundary layer flows over arbitrary topography and variations in effective/apparent aerodynamic roughness length (i.e., variations caused by microtopographic or vegetative roughness not resolved by the topographic model input to PHOENICS). In this study we used the PHOENICS k-ε closure scheme, which predicts the time-averaged properties of the flow. Our computational grid consisted of a 2-D terrain-following coordinate system with horizontal resolution of 1 m and a variable vertical distance ranging from 0.05 m to approximately 8 m, increasing with height above the bed. We used a uniform z_{0r} value of 0.01 m, i.e., a value appropriate for vigorous saltation conditions. However, nearly identical results were obtained using a z_{0r} value of 0.001 m (see section 4 for documentation of z_{0r} values in the range of 0.001–0.01 m for flow over erodible unvegetated beds under dune-forming conditions). We assumed a representative wind velocity, u, of 10 m s^{-1} at a reference elevation of 100 m above the bed. At the upwind boundary we assumed a logarithmic velocity profile consistent with $z_0 = 0.01$ m and $u = 10$ m s^{-1} at $z = 100$ m. A fixed

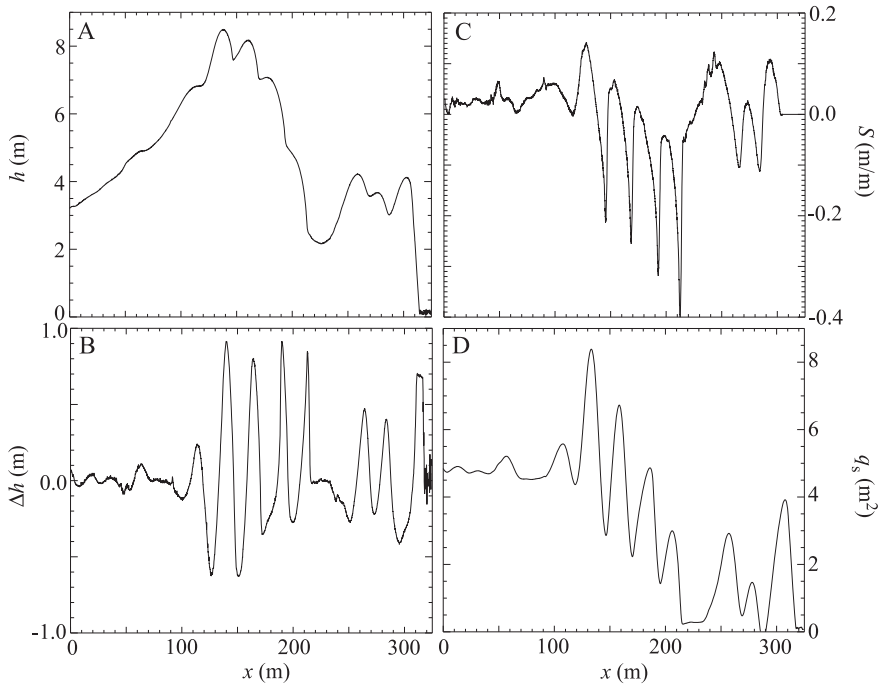

Figure 5. Products of the TLS surveys plotted along the transect shown in Figure 3b. Plots of (a) topographic elevation, h, as a function of distance, x, in the downwind direction, (b) topographic change, Δh, over the 3 month period between the two TLS surveys, (c) topographic slope, S, and (d) unit sediment flux, q_s, over the 3 month period.

pressure boundary condition was used at the downwind boundary. The model was run assuming neutrally buoyant atmospheric conditions; although strong stratification often occurs in deserts, atmospheric soundings [*Jerolmack et al.,* 2012] and ground observations [*Frank and Kocurek*, 1994] indicate that the ABL is well mixed under sand-transporting wind conditions at White Sands.

Aeolian sediment fluxes depend on both the bed shear stress and the local topographic slope. The threshold of entrainment is a function of the local slope [*Howard*, 1977; *Iversen and Rasmussen*, 1999], i.e.,

$$f_s = \frac{S_c + \frac{\Delta h_i}{\Delta x}}{S_c\sqrt{\left(\frac{\Delta h_i}{\Delta x}\right)^2 + 1}}, \tag{6}$$

where f_s is the relative difference between the threshold of entrainment on a sloping surface and the threshold of entrainment for the same grains on a flat surface and S_c is the tangent of the angle of internal friction (approximately 0.65 for well-sorted and rounded particles). The primary effect of equation (6) is to increase the flux of sand on lee slopes that are sloping at angles close to the angle of internal friction. On these lee slopes bed shear stresses are relatively low due to flow separation/recirculation, but gravitationally driven grain flows become a significant driver of sediment flux.

We assume that the unit sediment flux is proportional to the excess bed shear stress to the 1.5 power [*Bagnold*, 1941], i.e.,

$$q_s \propto (\tau_b - \tau_{b0})^{1.5}, \tag{7}$$

where τ_{b0} is the threshold bed shear stress for entrainment. Implementing equation (7) requires that we quantify the bed shear stress for a range of wind conditions to determine which wind storms caused transport and on which portions of the dune (depending on the slope dependence of τ_{b0}). In this study we used an approximate approach to quantifying the relative spatial variations in aeolian sediment flux that does not require individual wind events to be resolved. This approach uses the Taylor approximation

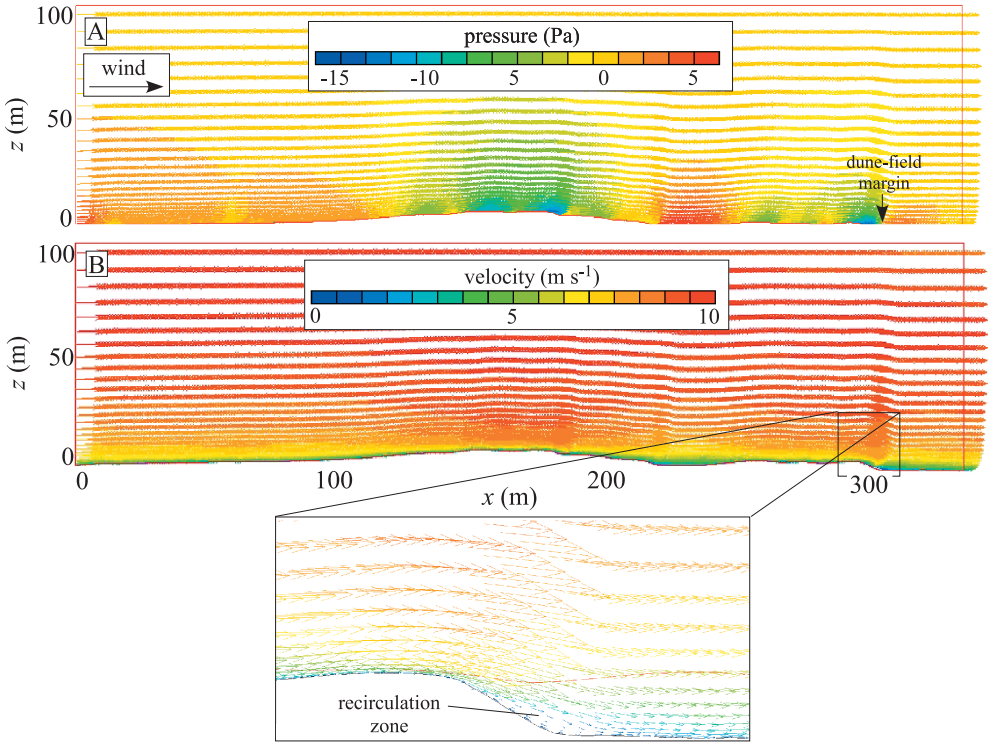

Figure 6. Color plots of (a) pressure and (b) velocity predicted by the PHOENICS CFD model for boundary layer flow over the topography of the dune complex along the transect shown in Figure 3.

$$1 - \frac{\tau_{b0}}{\tau_b} \approx \frac{\tau_b}{\tau_{b0}} \tag{8}$$

to approximate equation (7) as

$$q_s \propto \left(\frac{\tau_b}{f_s}\right)^{1.5}. \tag{9}$$

We scaled the maximum value of q_s predicted by equation (9) to match the maximum value of q_s measured in the field using the multitemporal TLS data (i.e., 8.4 m^2 over the 3 month time interval between surveys, measured at the crest of the dune complex). This procedure yielded a coefficient of proportionality in equation (9) equal to 27.3 $m^2\,Pa^{-1.5}$.

In order to test the hypothesis that the abruptness and stability of the downwind dune field margin is a result of a rough-to-smooth aerodynamic transition, we also used PHOENICS to model the 2-D boundary layer flow over flat terrain with a rough-to-smooth aerodynamic roughness transition from $z_{01} = 0.2$ m to $z_{02} = 0.01$ m (the subscript 01 refers to the surface upwind of the transition, and 02 refers to the value downwind of the transition). For comparison, we modeled the bed shear stress corresponding to a smooth-to-rough transition with the same effective roughness values. The computational grid for these roughness transitions was expanded to a maximum height of 300 m. We verified the robustness of the model predictions with respect to the grid resolution and the choice of maximum/reference height.

3.4. Ground-Penetrating Radar

We conducted a continuous, high-resolution subsurface survey of the transect shown in Figure 3B on March 6, 2013 using a digital GSSI SIR3000 impulse radar system with a 400 MHz transducer. The locations of radar traces were determined by Global Positioning System (GPS) measurements acquired approximately every 50 m along the transect using a handheld GPS with a spatial resolution of 3–4 m. Additionally, the odometer wheel provided continuous distance reading at 1 m intervals. Ground-penetrating radar (GPR) calibration was completed for gypsum sand above the water table by burying a marker to a depth of 0.3 m and identifying the marker at depth during initial scanning. We used the GSSI RADAN 7 software to process the

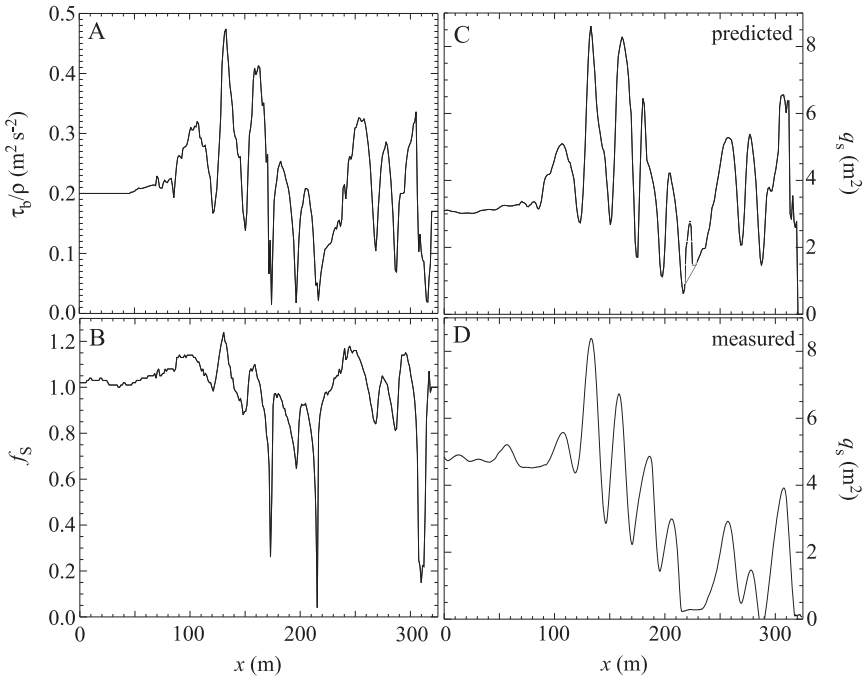

Figure 7. Comparison of predicted versus measured unit sediment fluxes, along with bed shear stress and the slope factor used to predict unit sediment flux. Plot of (a) relative bed shear stress versus horizontal distance along the predominant direction of aeolian transport, (b) the slope factor (equation (6)), (C) the model-predicted unit sediment flux (equation (9)) over the 3 month time period between 7 March and 4 June 2013, normalized to the maximum of the measured unit sediment flux data, and (d) measured unit sediment flux data over the 3 month time period (same as Figure 5d).

raw GPR profiles. Postprocessing included background removal, topographic correction, and raypath correction, as well as a time-varying gain adjustment to highlight subtle features.

4. Results

4.1. Terrestrial Laser Scanning and Creation of a DoD

Figure 3 illustrates the TLS-derived data as a shaded relief image of the topography on 4 June (Figure 3b) and as a DoD (Figure 3c) over the approximately 3 month interval between surveys. The DoD corresponds closely with the changes expected for dune migration under predominantly southwesterly winds, i.e., there is erosion on stoss sides and deposition on lee sides.

Figure 5 plots the elevation, slope, topographic change, and unit sediment flux along the transect shown in Figure 3b from the upwind (SW) to the downwind (NE) direction. At the scale of individual dunes, the unit sediment flux (Figure 5d) closely follows the bed slope, with increases in unit sediment flux along the profile occurring in zones of positive slope (stoss slopes) and decreases with distance occurring in zones of negative slope (lee slopes). At scales larger than individual dunes, the unit sediment flux varies in a way that does not correlate closely with local slope, however. Instead, the unit sediment flux declines systematically with distance toward the downwind margin. Given dunes of similar height, a decline in unit sediment flux is associated with a decline in dune migration rate. The decline in sediment flux with distance toward the margin is not perfectly systematic, i.e., the sediment flux increases slightly at the final dune. This increase may be associated with the fact that we chose to survey a portion of the dune margin characterized by a prominent unvegetated lobe. We will return to this point in section 5.

4.2. Field Measurements of Effective/Apparent Aerodynamic Roughness Length

Figure 4b presents the measurements of z_{0r} as a function of distance along the transect from a relatively vegetated interdune area to the unvegetated portions of the stoss side of the parabolic dune, along with 1σ uncertainties. Figure 4c presents the same data but as a plot of z_{0r} versus shear velocity u_* (data points collected in areas of higher vegetation density are shown using larger squares). The mean R^2 for the fits used to estimate

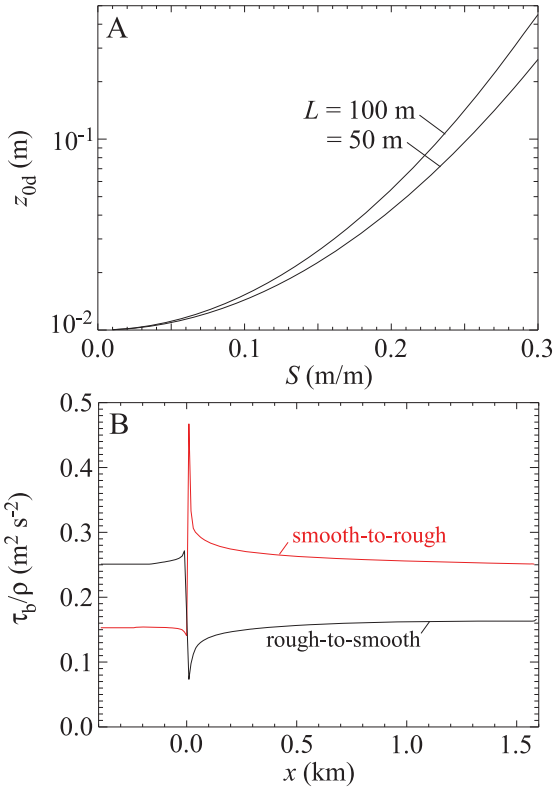

Figure 8. Results pertaining to a possible rough-to-smooth aerodynamic transition at the downwind dune field margin. (a) Estimate of the effective aerodynamic roughness length of a wavy surface (using equation (3)) with small-scale roughness z_{0r} = 0.01 m and for different values of the half width at half height, *L*, and maximum stoss-side slope, *S*. (b) PHOENICS model predictions of bed shear stress perturbations due to roughness steps with a smooth surface z_0 of 0.01 m and a rough surface z_0 of 0.2 m.

the 60 z_0 values is 0.967. These data demonstrate that z_{0r} is ~10^{-2}–10^{-1} m for vegetated surfaces of the saltbush/alkali sacaton association. On unvegetated surfaces, we measured z_{0r} values in the range of 10^{-5}–10^{-3} m. Such low values are not representative of dune-forming conditions, however, since active saltation can increase z_{0r} values by 1–3 orders of magnitude. The modified Charnock relation predicts z_{0r} in the range of 10^{-3}–10^{-2} m for shear velocities associated with vigorous saltation/dune-forming conditions. For this reason we adopted z_{0r} = 0.01 m as the default value for our calculations.

4.3. Numerical Modeling

Figure 6 illustrates color-coded vector maps of pressure and wind velocity predicted by the PHOENICS model for the actual topography of the dune complex, assuming the roughness parameters and boundary conditions identified in section 3. The inset image at the bottom illustrates that regions of flow separation are resolved in the model. Figure 7 demonstrates that the PHOENICS model produces spatial patterns of unit sediment flux that are similar to those we inferred from integration of the TLS-derived DoD values along the predominant transport direction. Figure 7a plots the raw bed shear stress predicted by PHOENICS. The bed shear stress exhibits a spatial pattern that is broadly consistent with the unit sediment flux, i.e., the flux is a maximum for the dune located at the crest of the dune complex and decreases systematically toward the dune margin except for a modest increase in flux over the last three dunes. Figure 7b plots the slope factor f_s required to account for the effect of bed slope on the sand transport threshold. The slope factor is close to 1.0 for most of the profile but decreases significantly on the lee sides of dunes as gravity becomes a dominant transport agent. The model-predicted unit sediment flux closely matches the measured unit sediment flux (Figure 7c) except that the model overpredicts the sediment flux for the last three dunes relative to the measurements. Overall, however, the correspondence between predicted and measured unit sediment fluxes is quite good considering that transport in the field occurs as a result of time-varying winds not explicitly accounted for in our analysis, as well as the fact that the model assumes a 2-D geometry.

As noted above, we measured the effective/apparent aerodynamic roughness length on a relatively flat, vegetated surface (analogous to the vegetated surface downwind of the margin) in White Sands to be in the range of 10^{-2}–10^{-1} m (Figure 5). To model the effects of a possible rough-to-smooth transition on the evolution of the downwind margin, we must also estimate the z_{0d} value of a wavy (i.e., dune-covered) surface. To do this, we used equation (4) with a z_{0r} value of 0.01 m and plotted the results corresponding to a range of values for the dune wavelength, λ, and maximum stoss-side slope, *S*. Figure 8a illustrates that the z_{0d} values estimated for the dune field using two representative values for dune half width at half height (*L* = 50 m and 100 m) and a range of values of maximum stoss-side slope up to 0.3 (16.7°). The results plotted in Figure 8a show that the z_{0d} values for the dune-covered surface increase from 0.01 m to a maximum of approximately 0.3 m for maximum stoss-side slopes comparable to those at White Sands. In this study we used 0.2 m as a representative z_{0d} value based on the *Jacobs* [1989] prediction plotted in

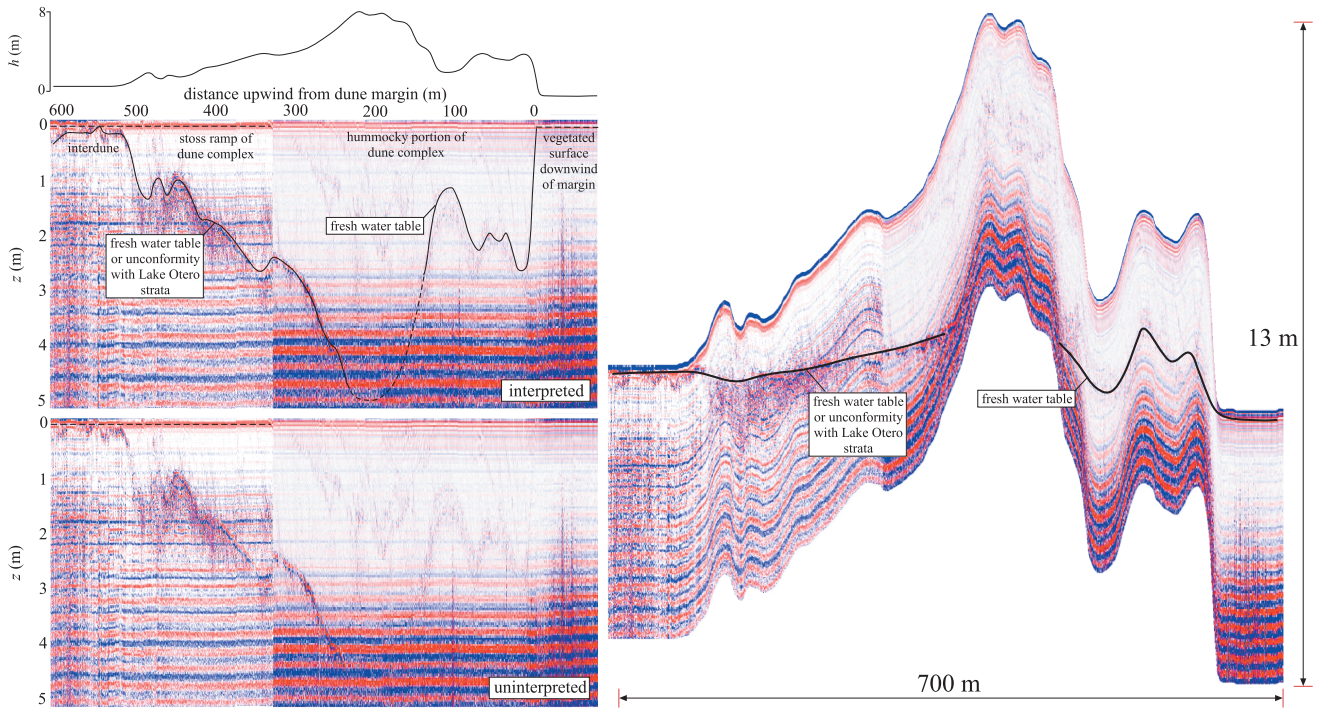

Figure 9. Results of the GPR survey (red indicates positive and blue indicates negative polarity) along the transect shown in Figure 3b (but extending farther upwind than the transect shown in Figure 3b). Also shown is the topographic profile along the transect. Interpreted data, uninterpreted data, and topographically corrected data are shown. We interpret the reflectors as representing a fresh water table. However, a reflection associated with an unconformity between the modern dune sands and Lake Otero strata cannot be ruled out on the western (upwind) side of the transect.

Figure 8a together with the results of J. D. Pelletier (in review, 2014), who computed effective aerodynamic roughness lengths for flow over dunes of different heights/slopes and found 0.2 m to be an appropriate estimate for z_{0d} at White Sands. Given that we measured effective roughness lengths in the range from 0.01 to 0.1 m on relatively flat, vegetated surfaces at White Sands, there may exist a modest rough-to-smooth transition at the downwind margin at White Sands, where the effective roughness goes from approximately 0.2 m on the unvegetated dunes to a value in the range of 0.01 to 0.1 m on the dune-free, vegetated surface downwind of the margin.

CFD models, however, indicate that any shear stress perturbation associated with a rough-to-smooth transition at the downwind margin of White Sands is likely to have only a minor effect, if any, on the sediment flux tens to hundreds of meters upwind of the transition. Figure 8b plots the bed shear stress associated with both a smooth-to-rough and a rough-to-smooth transition with a smooth surface roughness of $z_0 = 0.01$ m and a rough surface roughness of $z_0 = 0.2$ m. The smooth-to-rough transition generates a significant shear stress "overshoot," i.e., the shear stress immediately downwind of the transition reaches a maximum value almost twice as large as the asymptotic value achieved far downwind of the transition and stays significantly elevated for a distance of several hundred meters downwind. The analogous rough-to-smooth transition generates a shear stress undershoot that is less than half as large as the overshoot associated with the smooth-to-rough transition. Upwind from the rough-to-smooth transition there is a slight increase in the shear stress, i.e., the opposite of the effect we see in the data (i.e., a decrease in sediment flux and, by inference, bed shear stress on approach to the margin). These results suggest that any roughness transition at the downwind margin likely plays a minor role in controlling sediment fluxes in the vicinity of the margin.

4.4. GPR

The GPR survey reveals a reflector that follows the topography of the dune complex, increasing in both elevation and depth below the surface in areas of high and/or steep topography (Figure 9). We interpret this reflector to be the fresh groundwater table, although it could also correspond to an unconformity between modern sands and Lake Otero strata in the western (upwind) portion of the transect. Our interpretations are

informed by groundwater well observations that show that the fresh groundwater table increases in both elevation and depth below the surface within a dune complex adjacent to the downwind margin close to where we performed our GPR survey [*Newton and Allen*, 2014].

The significance of the results of the GPR survey for this study is twofold. First, the results demonstrate that the water table is relatively deep beneath the dune complex, and by inference, the sand within the higher portions of the dune complex is relatively dry and hence may be more mobile for otherwise similar wind forcing conditions. Drier conditions within the dune complex (compared with isolated parabolic dunes upwind and the dune-free vegetated surface downwind) are consistent with the remote sensing results of *Scheidt et al.* [2010]. Second, the GPR survey reveals no significant change in water table depth across the dune margin, other than that associated with the topographic changes accompanying the transition from the dune complex to a dune-free, vegetated surface. This indicates that groundwater and associated soil moisture effects are not likely responsible for the stability of the margin.

5. Discussion

The decrease in sediment flux on approach to the margin requires aggradation on the lee side of the dune complex, which likely contributes to the maintenance and/or growth of the dune complex. As *Bagnold* [1941] demonstrated, dune migration rates vary approximately in inverse proportion to their height. As such, the development of taller dunes/draas near the downwind margin naturally leads to a more stable (i.e., slowly migrating) margin.

Figure 1 demonstrates that the correlation between the dune margin and the formation of a dune complex is not perfectly one to one, i.e., there are portions of the dune margin that do not have an adjacent dune complex and there are dune complexes that exist at significant distances upwind from the margin. In places along the margin without a dune complex, heavily vegetated parabolics (i.e., plant spacing ~1 m throughout the dune) exist instead. In these areas, the feedback between dune stability and vegetation cover is likely the dominant effect in creating a stable margin. In this feedback, a minor decrease in sediment flux or dune migration rate can lead to a dramatic further reduction in dune mobility if the initial decrease in dune mobility facilitates vegetation growth on the dune (which further decreases mobility in a strong positive feedback) [*Yizhaq et al.*, 2009; *Barchyn and Hugenholtz*, 2012]. In places along the margin where a dune complex exists, this feedback between dune migration rate and vegetation cover undoubtedly plays a role in addition to, and acting in concert with, the aerodynamic effects documented here.

Scheidt et al. [2010] documented relatively dry sand conditions within the dune complex adjacent to the downwind margin compared with areas of lower long-wavelength topographic convexity, a result they associated with a 20% decrease in the threshold shear velocity in such areas. The results of our GPR survey are consistent with *Scheidt et al.* [2010]. Our results are also consistent with hydrologic investigations that show deeper water tables beneath taller and/or steeper portions of the dunes [*Newton and Allen*, 2014]. A decrease in water table depth and an associated increase in surface moisture on approach to the margin may contribute to the decrease in sediment flux we observe, in addition to the aerodynamic sheltering effect and vegetation-stabilization feedback discussed above.

The conceptual model illustrated in Figure 2 proposes that sediment flux decreases systematically on approach to the margin. The data collected in our survey area (Figure 3) mostly support this conceptual model, i.e., the sediment flux decreases systematically toward the margin in six out of the seven dunes. The terminal dune has a higher sediment flux than the three dunes upwind of it. We believe that this anomaly in our results is most likely a consequence of having chosen a survey area with a relatively unvegetated terminal dune. We chose this area because of its relative lack of vegetation (which improves the quality of the TLS and GPR surveys), but our choice has the downside that it may not be most representative of the behavior of the margin as a whole. The aerial photographs in Figure 1 indicate that the terminal dune in our survey area has been more active than adjacent portions of the margin over the past 70 years. As such, we believe that the anomalous behavior of this last dune does not disprove our proposed model but rather reflects local variability in margin migration. Additional multitemporal TLS data would be needed from other areas along the margin to resolve this issue.

The results of this paper demonstrate that a dune complex located near the downwind margin, once initiated, can be self-enhancing. We speculate that the decrease in sediment flux on approach to the margin leads to growth and/or maintenance of the dune complex, such that a taller and/or steeper dune complex leads to a greater difference in sediment flux between the stoss and lee sides, further increasing the height and/or slope of the complex. Future work could explore this hypothesis with landscape evolution models that couple boundary layer flow, sediment transport, and erosion/deposition over time scales of decades to millennia [e.g., *Durán et al.,* 2005, 2010; *Pelletier,* 2009; *Diniega et al.*, 2010].

The formation of dune complexes may contribute to the abruptness and stability of downwind dune field margins elsewhere, but proving so is more challenging than it may appear. Assessing the stability of a dune margin requires high-resolution aerial photographs separated by decades. Such imagery is most readily available (e.g., as a downloadable product) for areas within the U.S. We reconnoitered the dunes fields of the western U.S. using Google Earth but could find no downwind margin other than White Sands that was not significantly impacted by steep topography surrounding the dune field, fluvial channels, human activities, etc. Abrupt and relatively stable downwind margins are common (e.g., Algodones (CA), Kelso (CA), and Great Sand Dunes (CO)), but in all cases they are complicated by nonaeolian factors. As such, we cannot say at this time whether the mechanisms we identified as contributing to the abruptness and stability of the downwind margin at White Sands are operative at other downwind margins.

6. Conclusions

The downwind margin of the White Sands dune field is a relatively stable and abrupt transition to a dune-free vegetated surface. Repeat terrestrial laser scanning (TLS) surveys demonstrate that dunes of the dune complex adjacent to the downwind dune field margin migrate progressively more slowly as they approach the margin. We have shown how TLS-derived rates of erosion/deposition can be integrated along the predominant transport direction to obtain spatially continuous data for unit sediment flux. Computational fluid dynamics (CFD) modeling reproduces the first-order patterns of spatial variations in measured aeolian sediment flux and demonstrates that the decrease in sediment flux toward the dune field margin is due, in part, to the long-wavelength topography of the dune complex. In other words, dunes on the lee side of the dune complex are subjected to lower shear stresses as a result of the sheltering effect of the crest of the dune complex upwind. This work adds to a growing body of knowledge on how aeolian dunes are influenced by interactions among topography, boundary layer flow, and sediment transport at scales larger than individual dunes.

Acknowledgments

We wish to thank the students in the University of Pennsylvania GEOL305 course that assisted with the field data collection with D.J.J. and J.D.P. In particular, M. Domaracki led the GPR surveys. We also thank M. Hoose, who assisted with the June TLS survey as an REU student with J.D.P. J.D.P.'s work was partially supported by NSF EAR award 1323148. We are grateful for the access and logistical support provided by the White Sands National Monument staff, in particular D. Bustos. We wish to thank Associate Editor Doug Sherman and referees Ryan Ewing and Nick Lancaster for their very helpful reviews of the paper. All data are available upon request from J.D.P.

References

Ahlbrandt, T. S. (1979), Textural parameters of eolian deposits, in *A Study of Global Sand Seas*, edited by E. D. McKee, *U.S. Geol. Surv. Prof. Pap.*, *1052*, 21–51.

Andreotti, B., P. Claudin, and S. Douady (2002a), Selection of dune shapes and velocities. Part 1: Dynamics of sand, wind, and barchans, *Euro. Phys. J. B*, *28*, 321–339, doi:10.1140/epjb/e2002-00236-4.

Andreotti, B., P. Claudin, and S. Douady (2002b), Selection of dune shapes and velocities. Part 2: A two-dimensional modeling, *Euro. Phys. J. B*, *28*, 341–352, doi:10.1140/epjb/e2002-00237-3.

Bagnold, R. A. (1941), *The Physics of Blown Sand and Desert Dunes*, pp. 265, Methuen, London, U. K.

Baitis, E., G. Kocurek, V. Smith, D. Mohrig, R. C. Ewing, and A.-P. B. Peyret (2014), Definition and origin of the dune-field pattern at White Sands, New Mexico, *Aeolian Res.*, doi:10.1016/j.aeolia.2014.06.004.

Barchyn, T. E., and C. H. Hugenholtz (2012), Predicting vegetation-stabilized dune field morphology, *Geophys. Res. Lett.*, *39*, L17403, doi:10.1029/2012GL052905.

Bourke, M. C. (2010), Barchan asymmetry: Observations from Mars and Earth, *Icarus*, *205*, 183–197, doi:10.1016/j.icarus.2009.08.023.

Bridges, N. T., F. Ayoub, J.-P. Avouac, S. Leprince, A. Lucas, and S. Mattson (2012), Earth-like sand fluxes on Mars, *Nature*, *485*, 339–342, doi:10.1038/nature11022.

Brookfield, M. E. (1977), The origin of bounding surfaces in ancient aeolian sandstone, *Sedimentology*, *24*, 303–332.

Diniega, S., K. Glasner, and S. Byrne (2010), Long-time evolution of models of aeolian sand dune fields: Influence of dune formation and collision, *Geomorphology*, *121*, 55–68, doi:10.1016/j.geomorph.2009.02.010.

Durán, O., V. Schwämmle, and H. J. Herrmann (2005), Breeding and solitary wave behavior of dunes, *Phys. Rev. E*, *72*(2), 021308, doi:10.1103/PhysRevE.72.021308.

Durán, O., E. J. R. Partelli, and H. J. Herrmann (2010), A continuous model for sand dunes: Review, new developments and application to barchan dunes and barchan dune fields, *Earth Surf. Proc. Land.*, *35*, 1591–1600, doi:10.1002/esp.2070.

Ewing, R., and G. Kocurek (2010), Aeolian dune-field pattern boundary conditions, *Geomorphology*, *114*, 175–187, doi:10.1016/j.geomorph.2009.06.015.

Exner, F. M. (1920), Zur physik der dünen, *Akad. Wiss. Wien Math. Naturwiss. Klasse*, *129*(2a), 929–952.

Exner, F. M. (1925), Über die wechselwirkung zwischen wasser und geschiebe in flüssen, *Akad. Wiss. Wien Math. Naturwiss. Klasse*, *134*(2a), 165–204.

Feagin, R. A., A. M. Williams, S. Popescu, J. Stukey, and R. A. Washington-Allen (2012), The use of terrestrial laser scanning (TLS) in dune ecosystems: The lessons learned, *J. Coast. Res.*, doi:10.2112/JCOASTRES-D-11-00223.1.

Frank, A., and G. Kocurek (1994), Effects of atmospheric conditions on wind profiles and aeolian sand transport with an example from White Sands National Monument, *Earth Surf. Proc. Land.*, *19*, 735–745.
Havholm, K. G., and G. Kocurek (1988), A preliminary study of the dynamics of a modern draa, Algodones, southeastern California, USA, *Sedimentology*, *35*, 649–669.
Herrmann, H. J., G. Sauermann, and V. Schwämmle (2005), The morphology of dunes, *Physica A*, *358*, 30–38, doi:10.1016/j.physa.2005.06.004.
Herrmann, H. J., O. Durán, E. J. R. Parteli, and V. Schatz (2008), Vegetation and induration as sand dunes stabilizators, *J. Coast. Res.*, *24*, 1357–1368, doi:10.2112/08A-0011.1.
Hersen, P. (2004), On the crescentic shape of barchans, *Eur. Phys. J. B*, *37*, 507–514, doi:10.1140/epjb/e2004-00087-y.
Hersen, P., and S. Douady (2005), Collision of barchans as a mechanism of size regulation, *Geophys. Res. Lett.*, *32*, L21403, doi:10.1029/2005GL024179.
Hersen, P., K. H. Andersen, H. Elbelrhiti, B. Andreotti, P. Claudin, and S. Douady (2004), Corridors of barchans: Stability and size selection, *Phys. Rev. E*, *69*, 011304, doi:10.1103/PhysRevE.69.011304.
Hodge, R., J. Brasington, and K. Richards (2009), In situ characterization of grain-scale fluvial morphology using Terrestrial Laser Scanning, *Earth Surf. Proc. Land.*, *34*, 954–968.
Howard, A. D. (1977), Effect of slope on the threshold of motion and its application to orientation of wind ripples, *Geol. Soc. Am. Bull.*, *88*, 853–856, doi:10.1130/0016-7606(1977)88<853:EOSOTT>2.0.CO;2.
Iversen, J. D., and K. R. Rasmussen (1999), The effect of wind speed and bed slope on sand transport, *Sedimentology*, *46*, 723–731, doi:10.1046/j.1365-3091.1999.00245.x.
Jacobs, S. J. (1989), Effective roughness length for turbulent flow over a wavy surface, *J. Phys. Oceanogr.*, *19*, 998–1010, doi:10.1175/1520-0485(1989)019<0998:ERLFTF>2.0.CO;2.
Jerolmack, D. J., R. C. Ewing, F. Falcini, R. L. Martin, C. Masteller, C. Phillips, M. D. Reitz, and I. Buynevich (2012), Internal boundary layer model for the evolution of desert dune fields, *Nat. Geosci.*, *5*, 206–209, doi:10.1038/ngeo1381.
Katsuki, A., H. Nishimori, N. Endo, and K. Taniguchi (2005), Collision dynamics of two barchans simulated using a simple model, *J. Phys. Soc. Jpn*, *74*(2), 538–541, doi:10.1143/JPSJ.74.538.
Kocurek, G., M. Carr, R. Ewing, K. G. Halholm, and A. K. Singhvi (2007), White Sands Dune Field, New Mexico: Age, dune dynamics and recent accumulations, *Sediment. Geol.*, *197*, 313–331, doi:10.1016/j.sedgeo.2006.10.006.
Laick, M. M. (2001), Dune front movement trends at White Sands, New Mexico, Unpublished MS thesis, 124 pp., New Mexico State Univ., Las Cruces, New Mexico.
Langford, R. P. (2003), The Holocene history of the White Sands dune field and influences on eolian deflation and playa lakes, *Quat. Int.*, *104*, 31–39, doi:10.1016/S1040-6182(02)00133-7.
Langford, R. P., K. M. Pearson, K. A. Duncan, D. M. Tatum, L. Adams, and P.-A. Depret (2008), Eolian topography as a control on deposition incorporating lessons from modern dune seas: Permian Cedar Mesa sandstone, SE Utah, USA, *J. Sediment. Res.*, *78*, 410–422, doi:10.2110/jsr.2008.045.
Ludwig, J. C. (2011), *PHOENICS-VR Reference Guide*, CHAM Ltd., London, U. K. [Digital document Available at http://www.cham.co.uk/documentation/tr326.pdf.]
McKee, E. D. (1966), Structures of dunes at White Sands National Monument, New Mexico (and a comparison with structures of dunes from other selected areas), *Sedimentology*, *7*, 3–69, doi:10.1111/j.1365-3091.1966.tb01579.x.
McKee, E. D., and J. R. Douglass (1971), Growth and movement of dunes at White Sands National Monument, New Mexico, *U.S. Geol. Surv. Prof. Pap., 750-D*, 108–114.
Nagihara, S., K. R. Mulligan, and W. Xiong (2004), Use of a three-dimensional laser scanner to digitally capture the topography of sand dunes in high spatial resolution, *Earth Surf. Proc. Land.*, *29*, 391–398.
Newton, B. T., and B. Allen (2014), Hydrologic investigation at White Sands National Monument, *Open File Rep., 559*, New Mexico Bureau of Geology and Mineral Resources, 58 p.
Parteli, E. J., and H. J. Herrmann (2007), Dune formation on the present Mars, *Phys. Rev. E*, *76*, 041307, doi:10.1103/PhysRevE.76.041307.
Pelletier, J. D. (2009), Controls on the height and spacing of eolian ripples and transverse dunes: A numerical modeling investigation, *Geomorphology*, *105*, 322–333, doi:10.1016/j.geomorph.2008.10.010.
Pelletier, J. D. (2013), Deviations from self-similarity in barchan form and flux: The case of the Salton Sea dunes, California, *J. Geophys. Res. Earth Surf.*, *118*, 2406–2420, doi:10.1002/2013JF002867.
Reitz, M. D., D. J. Jerolmack, R. C. Ewing, and R. L. Martin (2010), Barchan-parabolic dune pattern transition from vegetation stability threshold, *Geophys. Res. Lett. 37*, L19402, doi:10.1029/2010GL044957.
Scheidt, S., M. Ramsey, and N. Lancaster (2010), Determining soil moisture and sediment availability at White Sands Dune Field, New Mexico, from apparent thermal inertia data, *J. Geophys. Res.*, *115*, F02019, doi:10.1029/2009JF001378.
Sherman, D. J. (1992), An equilibrium relationship for shear velocity and apparent roughness length in aeolian saltation, *Geomorphology*, *5*, 419–431.
Sherman, D. J., and E. J. Farrell (2008), Aerodynamic roughness length over movable beds: Comparison of wind tunnel and field data, *J. Geophys. Res.*, *113*, F02S08, doi:10.1029/2007JF000784.
Worman, S. L., A. B. Murray, R. Littlewood, B. Andreotti, and P. Claudin (2013), Modeling emergent structures of barchans dune fields, *Geology*, *41*, 1059–1062, doi:10.1130/G34482.1.
Yizhaq, H., Y. Ashkenazy, and H. Tsoar (2009), Sand dune dynamics and climate change: A modeling approach, *J. Geophys. Res.*, *114*, F01023, doi:10.1029/2008JF001138.